inorganics

MDPI

Article

Supramolecular Frameworks and a Luminescent Coordination Polymer from New β-Diketone/Tetrazole Ligands

Delia Blasi, Pierluigi Mercandelli and Lucia Carlucci *

Dipartimento di Chimica, Università degli Studi di Milano, via Camillo Golgi 19, 20133 Milano, Italy; delia.blasi@unimi.it (D.B.); pierluigi.mercandelli@unimi.it (P.M.)
* Correspondence: lucia.carlucci@unimi.it

Abstract: Mixed multidentate linkers with donor groups of different types can be fruitfully exploited in the self-assembly of coordination polymers (CPs) and Metal-Organic Frameworks (MOFs). In this work we develop new ligands containing a β-diketone chelating functionality, to better control the stereochemistry at the metal center, and tetrazolyl multidentate bridging groups, a combination not yet explored for networking with metal ions. The new ligands, 1,3-bis(4-(1*H*-tetrazol-5-yl)phenyl)-1,3-propanedione ($H_3\mathbf{L^1}$) and 1-phenyl-3-(4-(1*H*-tetrazol-5-yl)phenyl)-1,3-propanedione ($H_2\mathbf{L^2}$), are synthesized from the corresponding nitrile precursors by [2+3] dipolar cycloaddition of azide under metal-free catalytic conditions. Crystal structure analysis evidences the involvement of tetrazolyl fragments in multiple hydrogen bonding giving 2D and 1D supramolecular frameworks. Reactivity of the new ligands with different metal salts indicates good coordinating ability, and we report the preparation and structural characterization of the tris–chelate complex $[Fe(H\mathbf{L^1})_3]^{3-}$ (**1**) and the homometallic 2D CP $[Zn\mathbf{L^2}(DMSO)]$ (**2**). In compound **1** only the diketonate donor is used, whereas the partially deprotonated tetrazolyl groups are involved in hydrogen bonding, giving rise to a 2D supramolecular framework of (6,3)IIa topological type. In compound **2** the ligand is completely deprotonated and uses both the diketonate donor (chelating) and the tetrazolate fragment (bridging) to coordinate the Zn(II) ions. The resulting neutral 2D network of **sql** topology shows luminescence in the solid state, which is red shifted with respect to the free ligand. Interestingly, it can be easily exfoliated in water to give a luminescent colloidal solution.

Keywords: coordination polymers; 5-tetrazolyl ligands; β-diketone ligands; hydrogen bonded supramolecular frameworks; luminescence

Citation: Blasi, D.; Mercandelli, P.; Carlucci, L. Supramolecular Frameworks and a Luminescent Coordination Polymer from New β-Diketone/Tetrazole Ligands. *Inorganics* **2022**, *10*, 55. https://doi.org/10.3390/inorganics10040055

Academic Editors: Lars Öhrström, Susan Bourne and Francoise M. Amombo Noa

Received: 28 March 2022
Accepted: 16 April 2022
Published: 18 April 2022

1. Introduction

In the early nineties, the rational combination of multi-dentate bridging ligands with metal ions or clusters offered a new perspective to coordination chemistry, allowing the development of a new class of crystalline functional materials known as coordination polymers (CPs) and metal-organic frameworks (MOFs) [1,2]. Since then, there has been an enormous development in the field, as demonstrated by the achievement of a very large number of different materials and topologies, the study of a manifold of properties, as well as by the improvement of synthetic procedures enabling better control of the structure-properties relationship [3–6]. Fields of application and study of CPs/MOFs include, among others, gas storage and separation [7,8], catalysis [9,10], chemical sensing [11], drug delivery [12], CO_2 capture and conversion [13,14], environmental remediation [15,16], and water harvesting [16].

Many CPs and MOFs are assembled under solvothermal conditions from polycarboxylate linkers and metal ions or metal cluster nodes [3]. Nitrogen donor linkers are also widely used in the field, and among them, azolates allow to obtain porous and stable frameworks [17–19]. Tetrazole is a five-membered ring containing four nitrogen atoms, and has an acidity comparable to that of carboxylic acids. It is largely used as a synthetic

scaffold in different fields of applications, ranging from medicinal chemistry [20] to material science [21,22].

Tetrazoles are very versatile ligands: their deprotonated form can use up to four nitrogen atoms and bridge up to four metal atoms through varied coordination modes [23], allowing the isolation of diverse topologies, as well as highly thermally and chemically stable frameworks [24,25]. The convenient synthetic procedure to tetrazoles by [2+3] cycloaddition of azide on organonitrile molecules [26], enabled the synthesis of many polytetrazole ligands, as well as the in situ generation of different tetrazolate coordination networks under hydrothermal or solvothermal conditions [27,28]. The 1*H*-tetrazol-5-yl group has also been introduced in species already containing other different donor groups, developing a whole class of multifunctional tetrazole-based ligands. Some examples have been reported in the literature, proving their usefulness and versatility in the construction of coordination networks with interesting properties [29–31]; however, these species have been considerably less investigated in comparison to polytetrazoles.

On this basis, we decided to develop new mixed tetrazole ligands to be employed in networking with metal salts. Exploiting the convenient [2+3] cycloaddition synthetic procedure to convert an organonitrile group to a tetrazole moiety and our long-term interest in diketonate ligands [32,33], we report here the synthesis and characterization of two new tetrazole/diketone mixed ligands and the study of their reactivity with some metal ions. Both donor groups have been extensively employed in coordination chemistry; however, to the best of our knowledge, ligands combining tetrazole and diketone functionalities have not yet been used to build CPs and MOFs.

Starting from two benzonitrile-substituted β-diketone ligands we present here the preparation of the two new ligands 1,3-bis(4-(1*H*-tetrazol-5-yl)phenyl)-1,3-propanedione ($H_3\mathbf{L^1}$) and 1-phenyl-3-(4-(1*H*-tetrazol-5-yl)phenyl)-1,3-propanedione ($H_2\mathbf{L^2}$) through the synthetic pathway reported in Scheme 1. The study of their reactivity towards metal ions enabled us to isolate single crystals of the iron(III) tris–chelate complex $[Fe(H\mathbf{L^1})_3]^{3-}$ and of the zinc(II) 2D coordination polymer $[Zn\mathbf{L^2}(DMSO)]$ of **sql** topology. In the solid state, the Fe(III) complex establishes a hydrogen-bonded supramolecular framework corresponding to a self-catenated 2D net of (6,3)IIa topological type. Photoluminescence measurements in the solid state show that the Zn(II) coordination polymer is emissive, with the emission maximum red-shifted with respect to the free ligand. Moreover, it can be easily exfoliated in water.

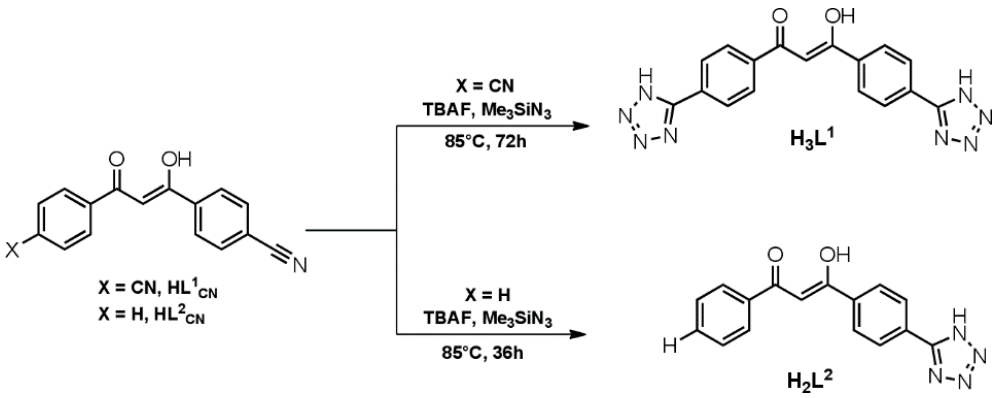

Scheme 1. Synthetic pathways to the new ligands $H_3\mathbf{L^1}$ and $H_2\mathbf{L^2}$.

2. Results and Discussion

2.1. Synthesis and Characterization

2.1.1. Synthesis of the Ligands $H_3\mathbf{L^1}$ and $H_2\mathbf{L^2}$

A common procedure for the synthesis of tetrazole-containing organic molecules is the well-established method introduced by Demko and Sharpless, consisting of a Zn(II) catalysed [2+3] dipolar cycloaddition reaction between an organonitrile and the azide

anion [26]. Accordingly, we decided to use as precursors for the new ligands the benzonitrile 1,3-disubstituted β-diketone molecules $H\mathbf{L}^{1}_{\mathbf{CN}}$ and $H\mathbf{L}^{2}_{\mathbf{CN}}$, and convert their nitrile groups to tetrazole through the [2+3] dipolar cycloaddition of azide; however, to avoid the use of metal ions as a catalyst, which often remain coordinated to the reaction product, we selected the metal-free and solventless procedure reported by Amantini et al. in 2004 [34]. In this procedure, the nitrile conversion occurs by reacting with trimethylsilylazide in the presence of tetrabutylammonium fluoride as a catalyst under mild heating. The synthetic pathways to obtain the new ligands $H_3\mathbf{L^1}$ and $H_2\mathbf{L^2}$ are reported in Scheme 1.

The new ligands have been isolated in good yields as pale-yellow solids and characterized by elemental analysis, ^{1}H and ^{13}C NMR and FT-IR spectroscopy. Furthermore, single crystals of the two molecules have been isolated and characterized by X-ray diffraction analysis.

Elemental analyses show that $H_3\mathbf{L^1}$ and $H_2\mathbf{L^2}$ precipitate with two and one clathrate water molecules, respectively. The FT-IR spectra for both ligands show the disappearance of the ν(C≡N) band at 2229 cm^{-1} and the presence of a series of bands between ca. 3460 and 2500 cm^{-1}, which are attributable to the stretching of N–H and O–H groups involved in hydrogen bonds. In the same region are also found aromatic C–H stretchings. Bands due to carbonyl groups of the enol moiety are found at ca. 1590 cm^{-1} for both ligands. In the region between ca. 1570 and 1480 cm^{-1}, C=C, C=N and N=N stretching vibrations are found. Skeletal ring vibrations for the tetrazole ring are present in the 1200–1010 cm^{-1} range. C–H bending and aromatic ring deformation–vibration bands are found in the range of ca. 990–700 cm^{-1} [35,36]. The IR spectra of $H_3\mathbf{L^1}$ and $H_2\mathbf{L^2}$ are reported in the Supporting Information (Figures S1 and S2).

^{1}H and ^{13}C NMR characterization for $H_3\mathbf{L^1}$ has been carried out in DMSO-d_6. The ^{1}H NMR spectrum shows a singlet at 7.57 ppm, which integrates for one hydrogen and is attributed to the C–H of the enol moiety, two doublets at 8.44 and 8.25 ppm for the phenyl hydrogens, and a broad signal at 16.98 ppm for the enol O–H proton. Due to fast exchange of the N–H with the adventitious water, its signal is not visible (Figure S3). In the ^{13}C NMR spectrum, the signal due to the carbon atom of the 5-tetrazolyl group is found at 155.74 ppm. Complete attribution of all carbon atoms is reported in Figure S4. ^{1}H and ^{13}C NMR characterization for $H_2\mathbf{L^2}$ has been performed in acetone-d_6. The C–H of the enol moiety is found at 7.37 ppm, whereas O–H and N–H protons are not detected [37,38]. Assignments for all protons are given in Figure S5. ^{13}C NMR spectra show the signal for the 5-tetrazolyl carbon atom at 157.33 ppm. The complete attribution of all carbon signals has been carried out by acquiring 2D homo and heteronuclear scalar correlation experiments (see Figures S6–S8).

2.1.2. Reactivity of $H_3\mathbf{L^1}$ and $H_2\mathbf{L^2}$ with Metal Ions

With the aim of preparing homo- and hetero-metallic networks, the reactivity of the two new ligands towards various metal salts has been first explored to isolate chelate monomers with available peripheral tetrazolyl groups. $H_3\mathbf{L^1}$ and $H_2\mathbf{L^2}$ have been reacted with Fe(III), Cr(III), Al(III), and Zn(II) salts in the presence of 1 eq. of base (NEt_4OH or NaOH) in ethanol or acetone as a solvent. In all cases, solid materials have been obtained and characterized by elemental analysis, FT-IR, and when possible, by ^{1}H NMR spectroscopy. All the data support the formation of chelate complexes. Nevertheless, it is difficult to quantify the number of deprotonated tetrazolyl groups and the overall anionic charge of the complexes. All the attempts to get single crystals to perform a structural analysis have not been successful. This has also been hampered by the low solubility of the products in common organic solvents. Moreover, their reactions with a second metal ion have given neither homo- nor hetero-metallic crystalline networks but unidentified powdered materials only. Despite these results, it has been possible to isolate single crystals of a tris–chelate complex of Fe(III) by stratifying an acetone solution of $FeCl_3$ on a solution of $H_3\mathbf{L^1}$ dissolved in THF and few drops of DMSO in the presence of NEt_4OH. By slow diffusion of the two solutions, in a few days, red block crystals are formed, which

are very unstable upon removal from the mother liquor. Nevertheless, X-ray diffraction analysis, performed at low temperatures, allows the elucidation of the crystal structure and a definition of the chemical formula of the compound as $[NEt_4]_3[Fe(H\mathbf{L^1})_3]\cdot 3THF$ (**1**). Crystal structure analysis suggests the presence of three N–H in the anionic complex involved in an intricate pattern of hydrogen bonds (*vide infra*). This species has been also synthesized in bulk under stirring, reacting Fe(III) chloride with 3 eq. of ligand in the presence of 1 eq. of NEt_4OH in acetone. From this reaction, a red solid is obtained whose FT-IR spectrum shows, in the 3400–2500 cm^{-1} region, the presence of many peaks attributable to N–H and C–H stretching vibrations; however, the elemental analysis does not give a clear evidence of the charge of the complex, that is the molar ratio between tetraethylammonium cations and the tris–chelate anion.

2.1.3. Synthesis and Characterization of the 2D Coordination Polymer $[Zn\mathbf{L^2}(DMSO)]$ (**2**)

In an attempt to crystallize the Zn(II) tris–chelate complex of the ligand $H_2\mathbf{L^2}$, pale-yellow block crystals of compound $[Zn\mathbf{L^2}(DMSO)]$ (**2**) have been isolated. X-ray diffraction analysis performed at room temperature shows that it is a homometallic neutral 2D coordination polymer, in which Zn(II) coordinates both the enolate and the tetrazolate moieties (*vide infra*). Compound **2** can be also easily prepared as a thin microcrystalline powder by reacting $H_2\mathbf{L^2}$ with $ZnCl_2$ and NaOH (stoichiometric ratio 1:1:3) in DMSO at room temperature, and by successive precipitation with water. The purity of this material is ascertained by comparison of its experimental powder diffraction pattern with that calculated from single-crystal X-ray diffraction data (Figure 1).

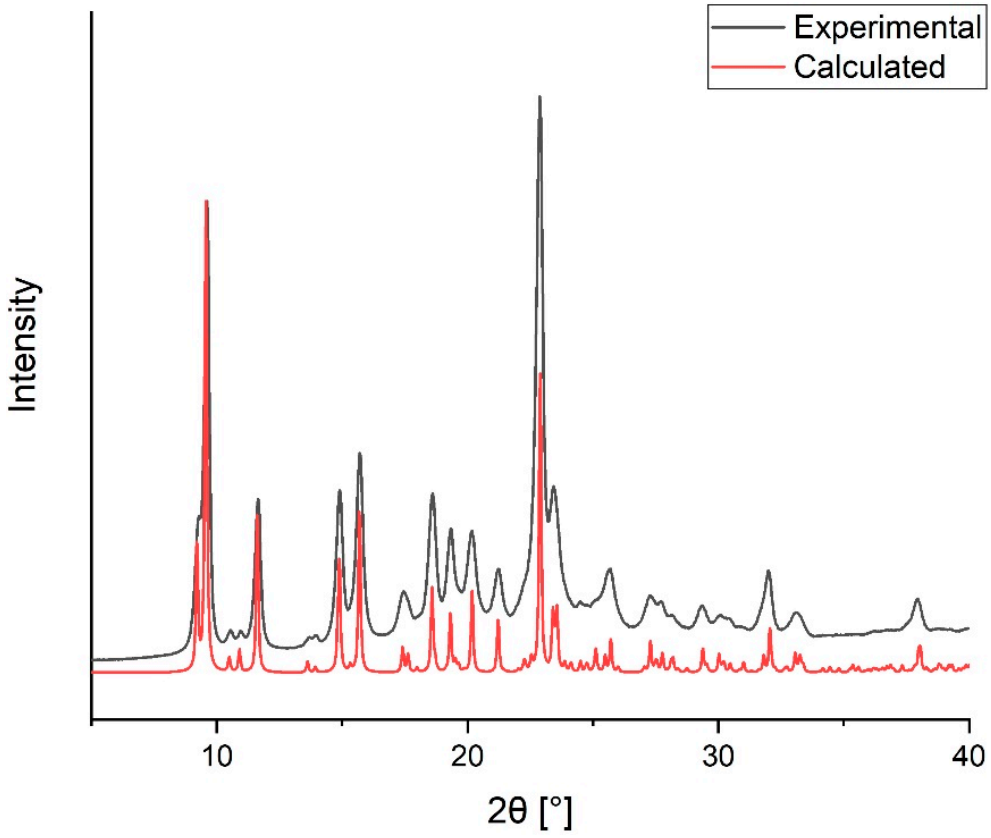

Figure 1. Comparison between experimental and calculated X-ray diffraction powder patterns for compound **2**.

The FT-IR spectrum of **2** shows the complete disappearance of N–H stretching frequencies in the 3460–2500 cm^{-1} range, whereas the presence of a residual weak band at ca. 3061 cm^{-1} can be attributed to the aromatic C–H stretching. The coordination of the enolate

fragment is supported by a small shift to low wavenumbers of the carbonyl stretching (from 1599 to 1595 cm^{-1}). The ν(S=O) stretching mode of the coordinated DMSO molecule is assigned to the peak at 1006 cm^{-1} (Figure 2). The shift to lower wavenumbers with respect to the corresponding value for free DMSO (1055 cm^{-1}) is in agreement with the κ*O* coordination mode of the molecule [36,39,40]. Thermal gravimetric analysis, performed under nitrogen, shows continuous weight loss starting from about 220 °C, suggesting that the loss of the coordinated DMSO molecules induces the subsequent decomposition of the species.

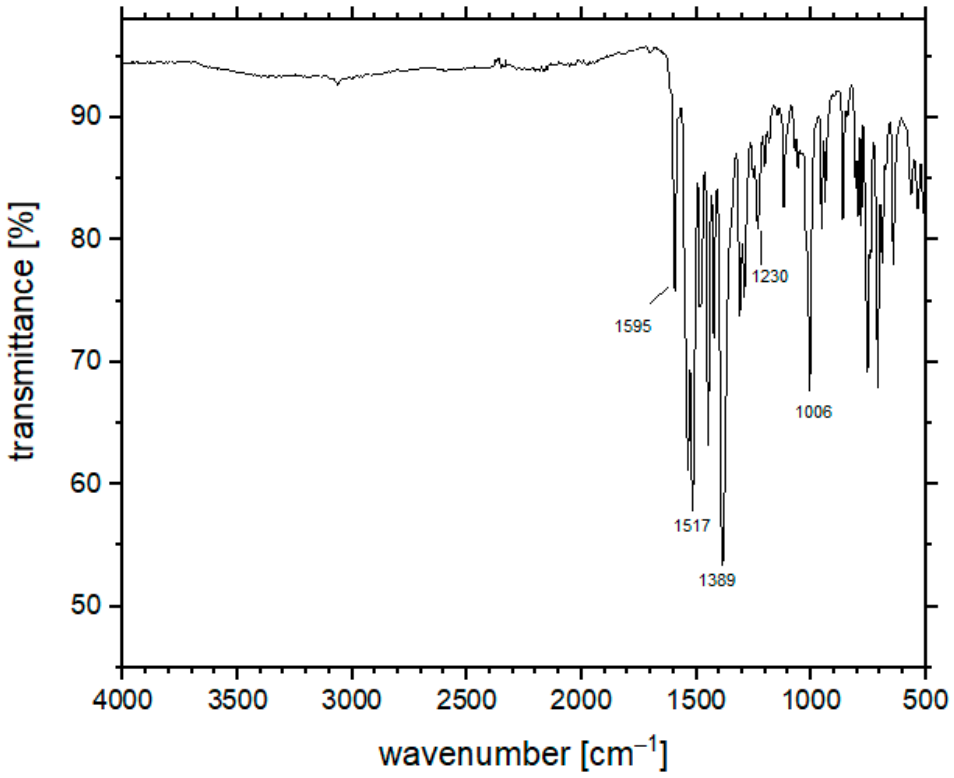

Figure 2. FT-IR spectrum of compound **2** collected in ATR mode.

The presence of Zn(II) d^{10} metal ions in the structure of **2** prompted us to investigate the photoluminescence in the solid state of both ligands and of the 2D coordination polymer. Photoluminescence measurements on the new ligands show very similar emission bands, with the emission maximum centered at 455 and 462 nm (λ_{exc} = 370 nm) for $H_3\mathbf{L^1}$ and $H_2\mathbf{L^2}$, respectively (Figure S9). As shown in Figure 3, upon excitation at 370 nm (the wavelength corresponding to the absorption maximum, see Figure S10) the emission of compound **2** shows a red shift with respect to the free ligand $H_2\mathbf{L^2}$, with a broad vibronically-unresolved band of charge–transfer character covering almost the entire portion of the visible region. The emission was also measured on a colloidal suspension of **2**, prepared by sonication-assisted exfoliation in water. A red shift with respect to the free ligand is also observed in this case, although it is lower than that observed in the solid state.

To characterize the exfoliated material, we performed an HR-TEM analysis which reveals the existence of thin free-standing 2D nanosheets of variable micrometric and sub-micrometric dimensions (Figure 4a,b). A fast–Fourier transformation pattern of a selected area of the sample confirms the maintenance of the crystalline nature of the material (Figure 4c).

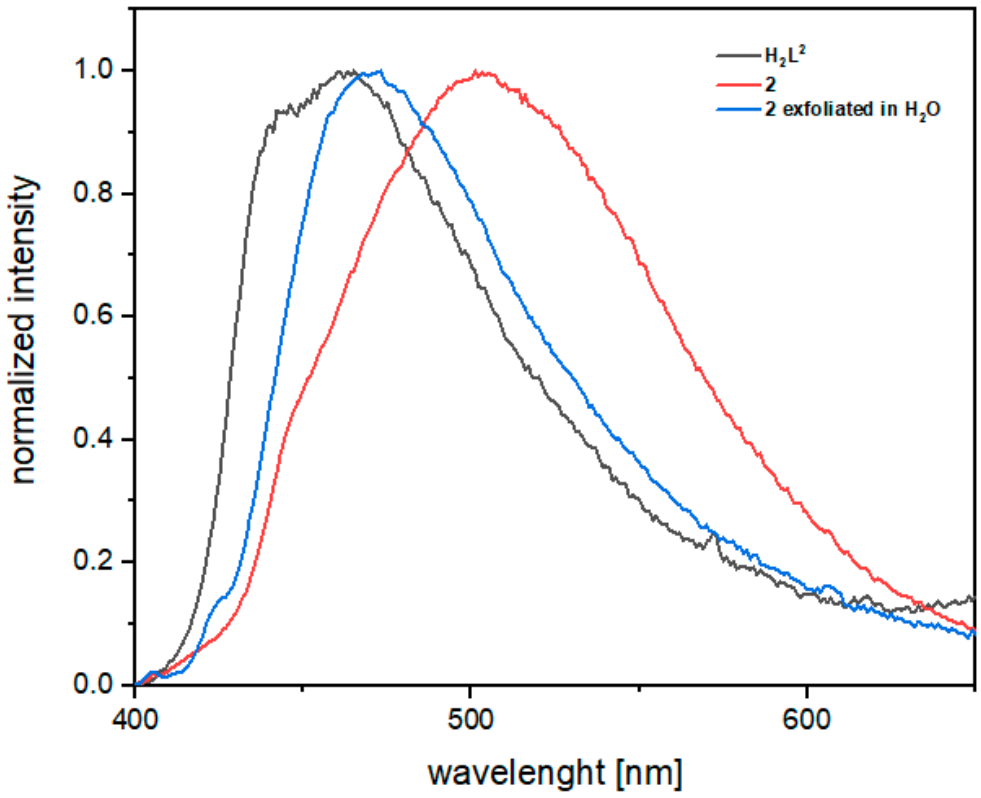

Figure 3. Emission spectra of the free ligand $H_2\mathbf{L^2}$, the coordination polymer **2** in the solid state and a suspension of **2** exfoliated in water (λ_{exc} = 370 nm).

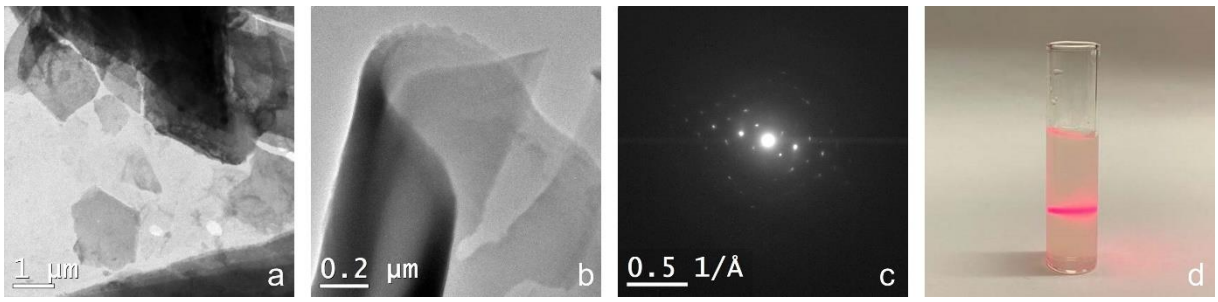

Figure 4. (**a**,**b**) HR-TEM images of the exfoliated **2** in water; (**c**) FFT pattern of a selected area; and (**d**) Tyndall effect of a water suspension of exfoliated **2**.

2.2. Crystal Structure Descriptions

2.2.1. Crystal Structure of $3H_3\mathbf{L^1}\cdot 2DMSO\cdot 4H_2O$

Single crystals of a solvate form of the neutral ligand $H_3\mathbf{L^1}$ have been isolated from a DMSO solution in the presence of a small amount of water. The ligand crystallizes in the *C*2/*c* space group of the monoclinic system with *Z* = 4. The asymmetric unit contains half an $H_3\mathbf{L^1}$ molecule lying on a two-fold axis (4*e* Wyckoff position) and one, one, and two molecules of $H_3\mathbf{L^1}$, DMSO and water, respectively, all laying in general positions, to give the overall formula $3H_3\mathbf{L^1}\cdot 2DMSO\cdot 4H_2O$ (Figure 5a). The asymmetric (A) and symmetric (B) $H_3\mathbf{L^1}$ molecules are both in the enol form with the O–H hydrogen equally disordered on the two oxygen atoms and engaged in intramolecular hydrogen bond (O1···O2 and O3···O3′ distances of 2.452(4) and 2.466(4) Å, respectively). The tetrazole hydrogen atoms are unequivocally positioned on the N^1 position of the five-membered rings and are all involved in hydrogen bonds. Leaving apart the tetrazole groups, both molecules A and B are quite flat, showing a maximum atomic displacement of 0.066(4) Å (molecule A) and 0.189(4) Å (molecule B) from the mean plane defined by the phenyl

and diketone/enol fragments. Tetrazoles are rotated with respect to this molecular mean plane, with dihedral angles of 16.95(5)° and 13.72(17)° in molecule A and 12.78(15)° in molecule B. Dihedral angles between tetrazole units are larger, at 28.4(2)° and 24.7(2)° for molecules A and B, respectively. The organization of the molecules in the solid state is governed by tetrazole/tetrazole and tetrazole/water hydrogen bonds (Figure 5b). In particular, the asymmetric molecule A is involved in two N1–H1···N8 [2.853(5) Å] and two O–H···N hydrogen bonds [O5–H26···N3 = 2.853(4) and N5—H12···O6 = 2.653(4) Å]. The symmetric molecule B is involved in two N–H···O [N9–H13···O5 = 2.608(4) Å] and two O–H···N [O6-H28···N11 = 2.869(4) Å] hydrogen bonds (Figure 5c). Every ligand then interacts with other four ligand molecules, either directly or through water molecules, and if all these hydrogen bonds are taken into account, a corrugated supramolecular layer perpendicular to the **c** direction is generated, showing a thickness of about 20 Å. Within a layer, all the carbonyl oxygen atoms are oriented in the same direction, which is reversed in adjacent layers through a center of inversion, resulting in an *ABAB* packing along **c** (Figure S11). DMSO molecules are located in the interlayer space, interacting with the layers by hydrogen bonding to water molecules [O5–H27···O4 = 2.678(4) and O6–H29···O4 = 2.707(4) Å]. The supramolecular layer is simplified to the **sql** topology, where the barycenter of the ligand is the 4-conn node whereas water molecules act as 2-conn linkers (Figure 5d).

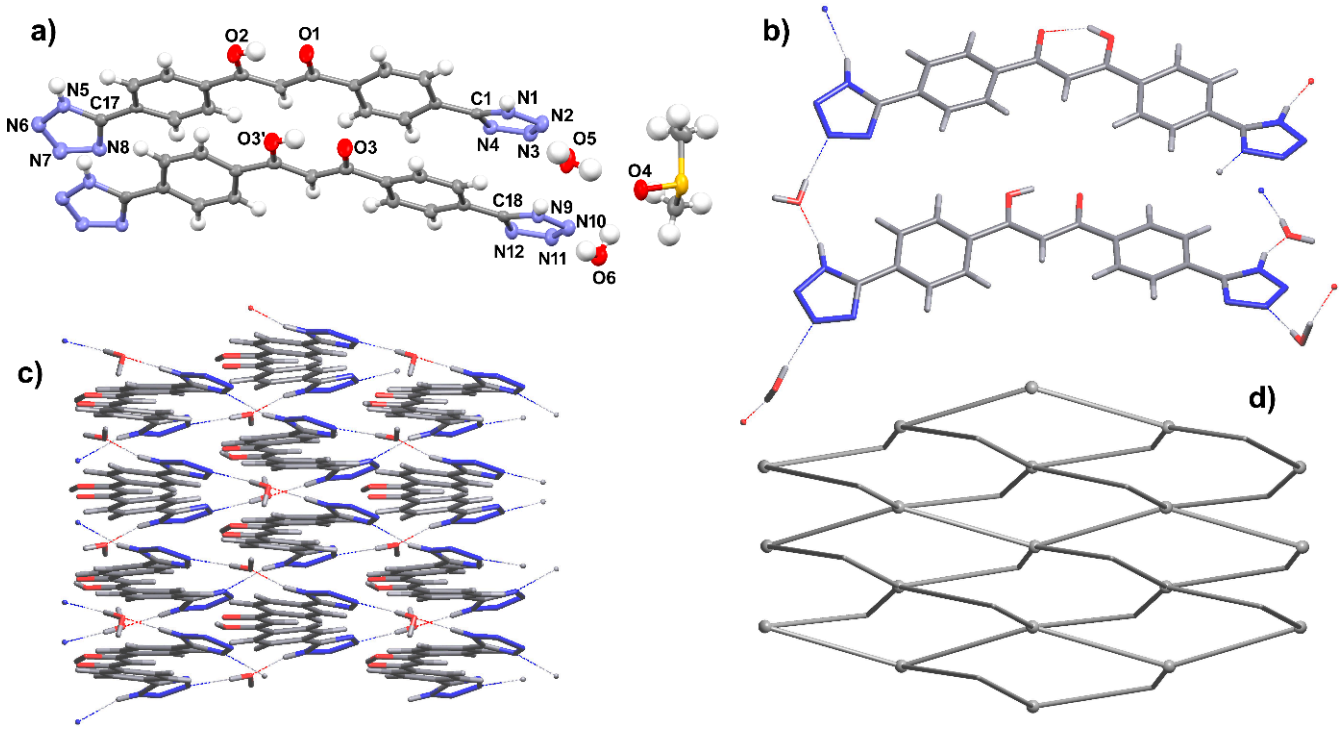

Figure 5. Crystal structure of $3H_3\mathbf{L^1}{\cdot}2DMSO{\cdot}4H_2O$. (**a**) ORTEP view of the asymmetric unit, showing molecules A and B with a partial labelling scheme; (**b**) view of the hydrogen-bonding pattern generating the supramolecular framework; (**c**) view along **c** of a supramolecular layer; (**d**) view of the simplified layer of **sql** topology. Ellipsoids at 50% level of probability. Symmetry code (′): $1 - x, y, {}^1/_2 - z$.

2.2.2. Crystal Structure of $H_2\mathbf{L^2}$

Crystals of $H_2\mathbf{L^2}$ have been isolated under hydrothermal conditions attempting its reaction with zinc nitrate. The molecule is in its enolic form and crystallizes in the $P2_1/c$ space group of the monoclinic system. The asymmetric unit contains only one molecule in a general position with $Z = 4$ (Figure 6a). The enol hydrogen is disordered over the two oxygen atoms and involved in an intramolecular hydrogen bond [O1···O2 = 2.4557(17)

Å]. With respect to $H_3\mathbf{L^1}$, here, the phenyl groups are more twisted with respect to the central diketone fragment and the maximum atomic displacement from the molecular mean plane (calculated excluding the tetrazole ring) is 0.253(1) Å, whereas the dihedral angle between this molecular plane and the tetrazole unit is 28.25(5)°. The molecules are organized through N1–H1A···N1 and N4–H1B···N4 intermolecular hydrogen bonds (N···N distances of 3.0070(16) and 3.0705(16) Å, respectively), so that every molecule interacts with two other molecules through the tetrazole hydrogen atom, which is equally disordered over the N^1 and N^4 positions of the five-membered ring. These hydrogen bonds give linear chains of tetrazole rings in which the molecules are directed outward on both sides of the chains and the carbonyl groups are oriented all in the same direction on one side, and in the opposite direction on the other side (Figure 6b). The chains run along the [1 1 0] and [1 −1 0] directions, superimpose along **a**, and pack through interdigitation (Figure 6c,d).

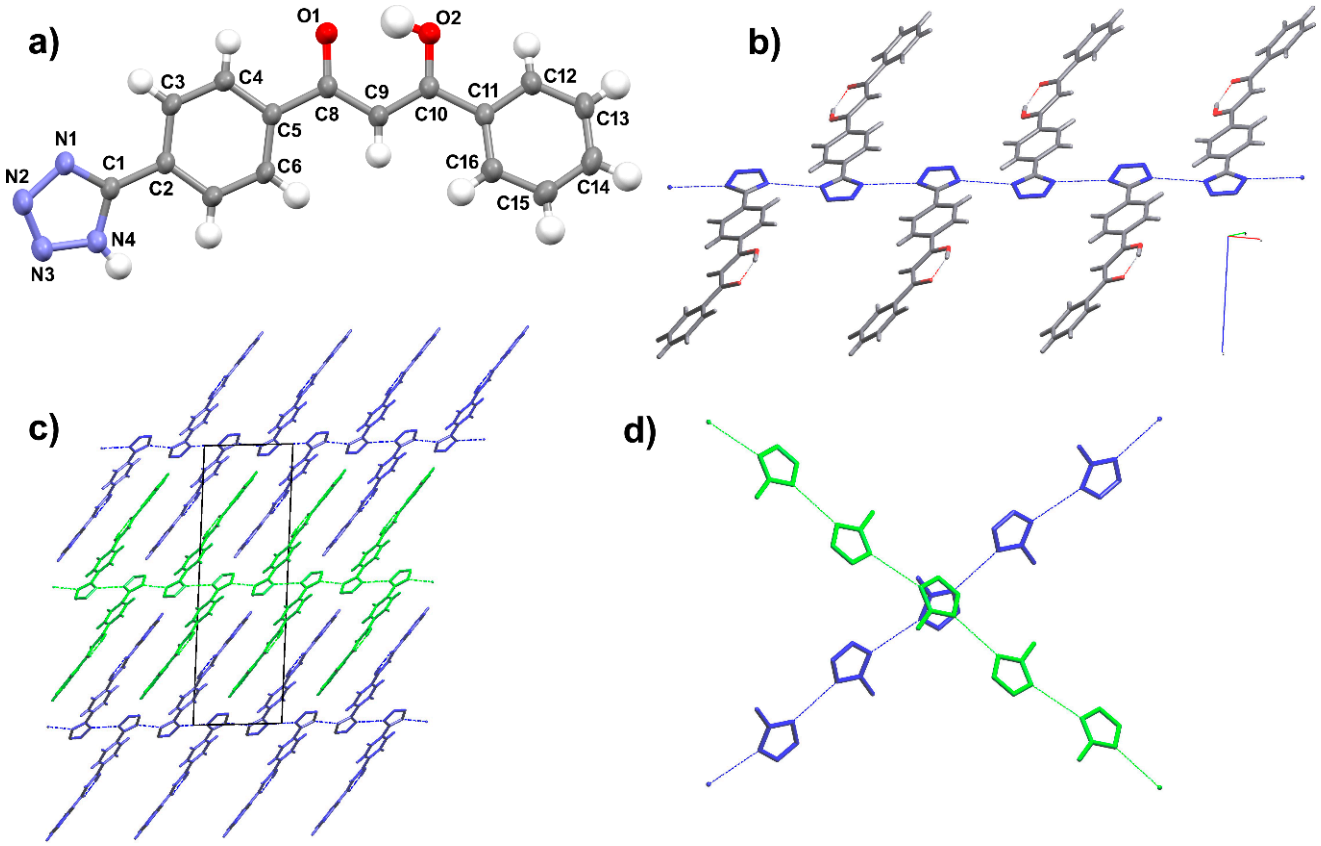

Figure 6. Crystal structure of $H_2\mathbf{L^2}$. (**a**) ORTEP view of the asymmetric unit, showing the labelling scheme; (**b**) view of a single linear chain; (**c**) view along **b**, showing molecular packing and interdigitation; (**d**) the two orientations adopted by the linear chains (only hydrogen-bonded tetrazole units are shown for clarity). Ellipsoids at 50% level of probability. Hydrogen atoms involved in hydrogen bonds are removed for clarity.

2.2.3. Crystal Structure of $[NEt_4]_3[Fe(H\mathbf{L^1})_3]\cdot 3THF$ (**1**)

Dark-red crystals of **1** are obtained by layering an acetone solution of $FeCl_3\cdot 6H_2O$ on $H_3\mathbf{L^1}$ dissolved in THF with small amounts of DMSO and NEt_4OH. The crystals are very unstable when removed from the mother liquor and single-crystal structure elucidation has been performed at 150 K. Compound **1** crystallizes in the *P*–1 space group of the triclinic system and the asymmetric unit contains one iron complex and three tetraethylammonium cations (Figure 7a). THF molecules are severely disordered and cannot be satisfactorily described by means of a discrete model. The amount of THF *per* formula unit has been

estimated by evaluation of the void space in the structure (835 Å^3), with respect to the volume occupied by a single THF molecule (120–140 Å^3, from a survey of structures in the Cambridge Structural Database containing clathrate THF). The presence of three cations indicates that three of six peripheral tetrazole fragments are deprotonated. The quality of the diffraction data does not allow the unequivocal assigning of positions N^1 or N^2 to tetrazole hydrogens, however, the pattern of hydrogen bonds clearly shows that all six tetrazoles are involved in hydrogen bonds (Figure 7a). In the tris–chelate complex, the metal is in a slightly distorted octahedral environment with the Fe–O distances in the range 2.001(3)–1.974(2) Å, and the O–Fe–O angles in the ranges 85.48(11)–98.64(11)° and 171.70(12)–177.24(12)° for the *cis* and *trans* interactions, respectively.

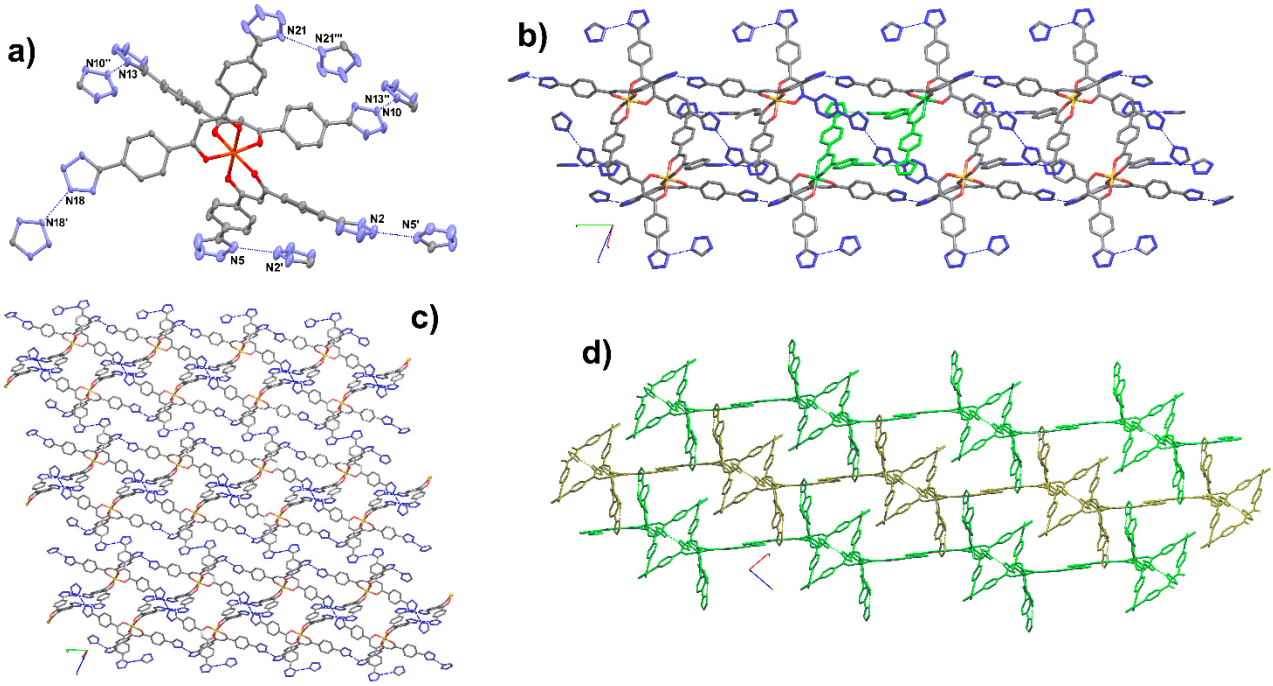

Figure 7. Crystal structure of $[NEt_4]_3[Fe(HL^1)_3]\cdot 3THF$ (**1**). (**a**) ORTEP view of the Fe(III) complex, showing the hydrogen-bonding pattern and a partial labelling scheme; (**b**) ladder motifs showing self-catenation through pseudo-rotaxane links: in green this is evidenced in the ring, and the blue shows the axle; (**c**) molecular view of a single layer; (**d**) view along **b** of the molecular packing. Ellipsoids at 30% level of probability. Symmetry code (′): $1-x, 1-y, 1-z$; (″): $x, 1+y, z$; (‴): $-x, 1-y, -z$.

All complexes are connected to each other by N–H···N hydrogen bonds to give a 2D supramolecular framework which can be described as being composed of ladders built up by N10···N13 = 2.669(6) Å and N21···N21 = 2.738(8) Å hydrogen bonds (Figure 7a,b). On the lateral chains of these ladders, the tris–chelate complexes show opposite chirality. Additional N18···N18 = 2.630(5) Å hydrogen bonds connect the ladders to give the overall 2D framework (Figure 7c,d). The layers are self-catenated through rings formed by N2···N5 = 2.629(8) Å hydrogen bonds. Simplification of the HB framework gives the 5-conn net of topological type (6,3)IIa with Point Symbol $\{4^8.6^2\}$ (Figure S12).

2.2.4. Crystal Structure of $[ZnL^2(DMSO)]$ (**2**)

Crystals of **2** suitable for single-crystal diffraction analysis have been initially isolated from a DMSO solution of the tris–chelate monomer $[Zn(HL^2)_3]^-$ stratified with pure THF after a few days. The compound crystallizes in the $P2_1/n$ space group of the monoclinic system. The asymmetric unit contains one zinc atom, one ligand molecule in its deprotonated form, and one DMSO molecule. Each zinc atom coordinates three different ligands

and one DMSO molecule, adopting a ZnO_3N_2 trigonal bipyramidal geometry. One ligand molecule interacts with three different metal atoms by chelation with the β-diketonate group to one of these, and by μ-κN^2:κN^3 coordination of its tetrazolate (ttz) moiety on the other two, generating [Zn_2(μ-ttz)$_2$] dinuclear units [Zn···Zn = 3.7078(12) Å]. Metal coordination is completed by a DMSO-κ*O* molecule disposed in *trans* to a diketonate oxygen atom (Figure 8a). The two nitrogen atoms are located on the equatorial plane of the trigonal bipyramid, together with an oxygen atom from the diketonate moiety, whereas in axial positions are located two oxygen atoms (one from DMSO and one from diketonate). The resulting structure is a 2D layer of **sql** topology in which the 4-conn nodes are the dinuclear zinc units, whereas phenyltetrazolate moieties are disposed along the edges of the square windows. The flat dinuclear [Zn_2(μ-ttz)$_2$] units adopt two different orientations which, in a single square window, are alternately disposed almost perpendicularly to each other. This arrangement gives rise to a thick layer, decorated on both sides by protruding phenyl groups and DMSO molecules (Figure 8b). The layers are perpendicular to the [1 0 1] direction and pack along this direction in an *ABAB* sequence. The dinuclear units of one layer lie in the center of windows belonging to adjacent layers. Phenyl groups and DMSO molecules point into the square channels visible along the crystallographic axis **a** (Figure 8c,d).

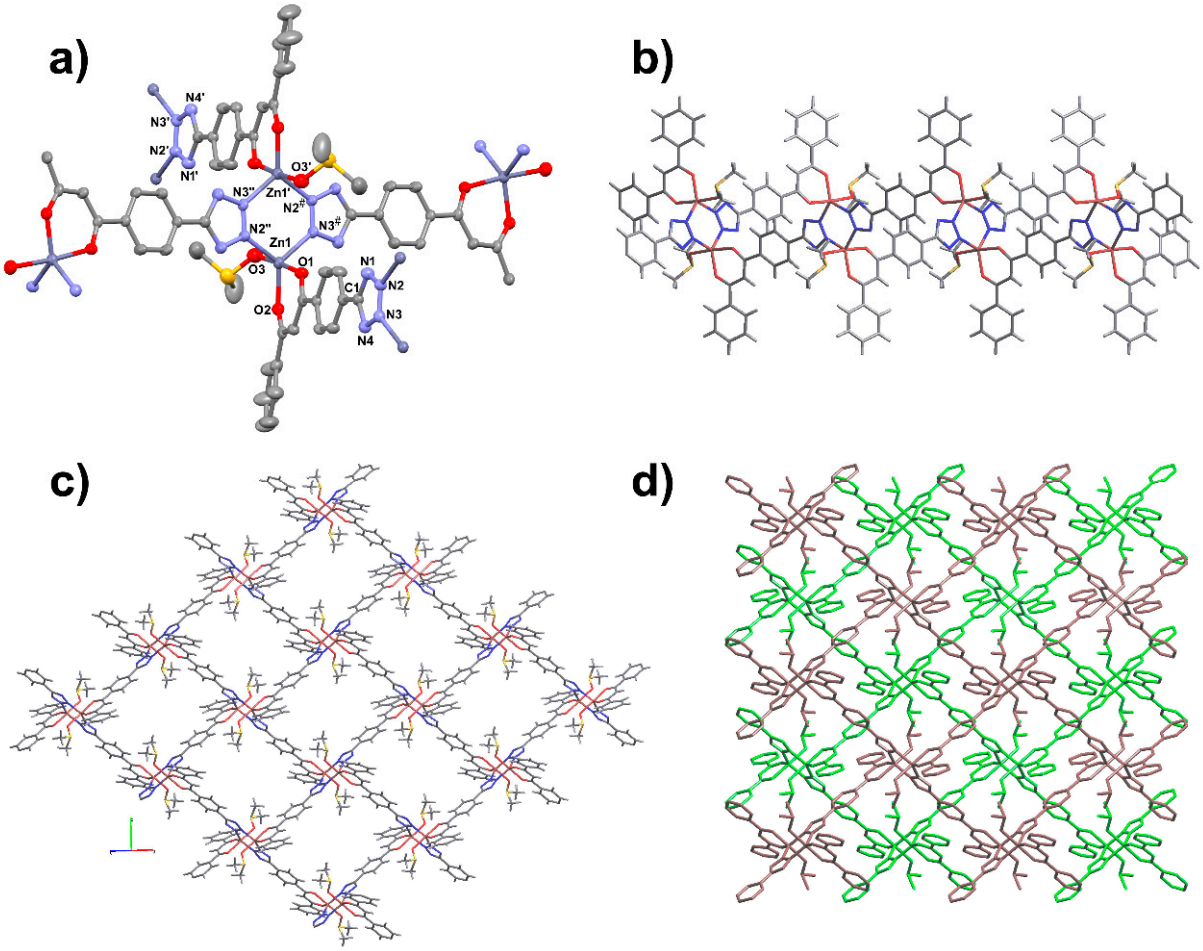

Figure 8. Crystal structure of [Zn**L**^{2}(DMSO)] (**2**). (**a**) ORTEP view of the coordination environment of the Zn(II) atoms; (**b**) lateral view along **b** of a single layer; (**c**) view of the layer along the (1 0 1) direction and (**d**) *ABAB* packing along the same direction. Ellipsoids at 50% level of probability. Symmetry code (′): –*x*, –*y*, –*z*; (″): 1/2 − *x*, 1/2 + *y*, –1/2 − *z*; (‴): –*x*, 1 − *y*, –*z*; (#): –1/2 + *z*, –1/2 − *y*, 1/2 + *z*.

3. Materials and Methods

All commercial reagents and solvents employed (Merck–Aldrich) are of high-grade purity and are used as supplied without further purification. All manipulations are performed under aerobic conditions. Starting ligands $H\mathbf{L}^1_{\mathbf{CN}}$ and $H\mathbf{L}^2_{\mathbf{CN}}$ are prepared according to literature procedures [32].

NMR spectra are recorded on a Bruker AC400 instrument; δ values are given in ppm relative to tetramethylsilane. Infrared spectra are collected on a Perkin–Elmer Frontier and Paragon 1000 FTIR spectrometers in ATR mode or in KBr. Thermal gravimetric analysis (TGA) is performed on a Perkin–Elmer TGA7 instrument under nitrogen with a temperature rate of 10 °C/min. Powder X-ray diffraction patterns are recorded on a Rigaku Miniflex diffractometer (Cu *Kα* radiation, λ = 1.5405 Å) in the 5–55° 2θ range (0.015° and 1 s per step). Elemental analyses are carried out at the Microanalytical Laboratory of the University of Milan with a Perkin–Elmer 2400 instrument. Fluorescence measurements are performed on a Horiba Fluorolog-3 spectrofluorometer. Exfoliation experiments are performed using the ultrasonic bath Branson 5510 at 135 W and an Eppendorf 5430 centrifuge. Absorption spectra are recorded at room temperature on an Agilent 8543 spectrophotometer using quartz cells with a 1.0 cm path length. HR-TEM images are acquired on a TECNAI FEG 200 kV.

3.1. Preparation of the Ligands and of the Complexes

3.1.1. Synthesis of $H_3\mathbf{L^1}$

In a Teflon reactor, the ligand $H\mathbf{L}^1_{\mathbf{CN}}$ (274.4 mg; 1.000 mmol) is added, as are tetrabutylammonium fluoride (315.7 mg; 1.001 mmol) and trimethylsilylazide (578.4 mg; 5.020 mmol). The Teflon reactor is closed in an autoclave and heated at 85 °C for 72 h. After cooling to RT, the mixture is poured into a beaker and added, under stirring, with 30 mL of acetone. After a few minutes, a dark yellow solid separates from a colorless solution, which is first recovered by filtration on a Büchner and successively dissolved in 15 mL of DMSO to give a yellow-orange solution. The solution is acidified with HCl 1 M and a pale-yellow solid precipitate. This solid is recovered by filtration, then suspended in a few milliliters of acetone and filtered again on a Büchner to give $H_3\mathbf{L^1}$ (yield: 58%). Analysis calculated for $C_{17}H_{16}N_8O_4$ (%): C, 51.51; H, 4.07; N, 28.27. Found: C, 51.24; H, 4.90; N, 27.82. ^{1}H NMR (400 MHz, DMSO-d_6) δ = 16.98 (s, broad, 1H), 8.44 (d, ^{3}J = 8.53 Hz, 4H), 8.25 (d, ^{3}J = 8.53 Hz, 4H), 7.57 (s, 1H). ^{13}C NMR (400 MHz, DMSO-d_6) δ = 184.78, 155.74, 128.95, 127.75, 136.98, 94.85. FT-IR (cm^{-1}) = 3465 br, 3358 m, 2615 m, 2501 m, 1582 m, 1530 m, 1493 m, 1432 m, 1293 m, 1240 m, 1154 w, 1129 s, 1091 s, 993 s, 904 m, 798 s, 732 m, 534 s, 488 s.

3.1.2. Synthesis of $H_2\mathbf{L^2}$

In a Teflon reactor, the ligand $H\mathbf{L}^2_{\mathbf{CN}}$ (700.2 mg; 2.809 mmol) is added, as are tetrabutylammonium fluoride (443.0 mg; 1.404 mmol) and trimethylsilylazide (808.6 mg; 7.019 mmol). The Teflon reactor is closed in an autoclave and heated at 85 °C for 37 h. After cooling to RT, the mixture is poured into a beaker and added with 15 mL of ethyl acetate and 15 mL of deionized water. The organic phase is separated in a separating funnel and further washed with 15 mL of ethyl acetate. The collected organic phase is then evaporated to dryness in a rotary evaporator, leaving a sticky product which is then dissolved in CH_2Cl_2 to give a yellow solution. This solution is added with HCl 1 M under vigorous stirring until there is complete precipitation of a yellow solid. The solid is recovered by filtration, washed with water, CH_2Cl_2, and then dried in air to give $H_2\mathbf{L^2}$ (yield: 77.1%). Analysis calculated for $C_{16}H_{14}N_4O_3$ (%): C, 61.93; H, 4.55; N, 18.06. Found: C, 61.70; H, 4.70; N, 18.20. ^{1}H NMR (400 MHz, acetone-d_6) δ = 8.37 (d, ^{3}J = 8.65 Hz, 2H), 8.31 (d, ^{3}J = 8.65 Hz, 2H), 8.20 (dd, ^{3}J = 7.28 Hz, ^{4}J = 1.30 Hz, 2H), 7.66 (tt, ^{3}J = 7.24 Hz, ^{4}J = 1.30 Hz, 1H), 7.58 (*pst*, ^{3}J = 7.24 Hz, ^{3}J = 7.28 Hz, 2H), 7.37 (s, 1H). ^{13}C NMR (400 MHz, acetone-d_6) δ = 186.69, 183.89, 157.33, 137.40, 135.29, 133.36, 128.85, 127.61, 127.43, 93.69. FT-IR (cm^{-1}) = 3446 br, 3328 br, 3219 w, 2569 w, 2497 w, 1962 w, 1599 m, 1589 m, 1564 s, 1523 s, 1495 s, 1458 m, 1404 m, 1287 m, 1228 s, 1133 s, 1092 m, 1014 m, 988 s. 862 m, 774 m, 748 s, 685 m, 628 m, 461 w.

3.1.3. Crystallization of $[NEt_4]_3[Fe(HL^1)_3]\cdot 3THF$ (**1**)

Compound **1** is isolated as block red crystals by slow diffusion of metal and ligand solutions in a test tube. In detail, H_3L^1 (5.0 mg; 0.014 mmol) is dissolved in THF (4 mL) and few drops of DMSO and added with 5.9 µL of a 35% water solution of NEt_4OH (0.014 mmol). This solution is stratified with an acetone solution (4 mL) of $FeCl_3\cdot 6H_2O$ (1.3 mg; 0.0048 mmol). The solutions are left to slowly diffuse at room temperature and red crystals of **1** are formed in a few days. Crystals of **1** are very unstable when removed from the mother liquor, due to the almost instantaneous loss of the THF clathrate molecules. Elemental analysis can be performed only on desolvated crystals. Analysis calculated for $C_{75}H_{90}FeN_{27}O_6$ (%): C, 59.20; H, 5.96; N, 24.86. Found: C, 59.37; H, 6.14; N, 24.55. FT-IR (cm^{-1}) = 3381 br, 2983 br, 2841 m, 2734 s, 1930 w, 1588 s, 1536 s, 1514 s, 1436 m, 1380 s, 1308 s, 1231 m, 1059 m, 994 m, 858 w, 795 m, 753 m, 657 w, 579 w.

3.1.4. Synthesis of $[ZnL^2(DMSO)]$ (**2**)

A solution of $ZnCl_2$ (23.3 mg, 0.170 mmol) in DMSO (1 mL) is slowly added when stirring H_2L^2 (50.0 mg, 0.170 mmol) dissolved in 1 mL of DMSO with 340 µL of aqueous NaOH (1 M, 0.340 mmol). A clear yellow solution is obtained which is left to react at room temperature for 24 h. Then, the mixture is treated with 5 mL of deionized water to induce the precipitation of the product as a microcrystalline pale-yellow powder. The solid is recovered by filtration on a Büchner, washed with 10 mL of water, and dried in air (yield: 80%). The purity of the product was confirmed by X-ray powder diffraction. Analysis calculated for $C_{18}H_{18}N_4O_4SZn$ (%): C, 47.85; H, 4.02; N, 12.40. Found: C, 47.63; H, 4.07; N, 12.05. FT-IR (cm^{-1}) = 1595 s, 1538 s, 1517 s, 1484 s, 1389 s, 1310 w, 1290 w, 1230 w, 1120 w, 1006 s, 953 w, 863 w, 795 w, 756 m, 709 m, 644 w, 533 w (Figure 2). The preparation of the corresponding exfoliated material is performed employing the solvent-induced delamination method [41]. Five mg of **2** are suspended in 5 mL of water and sonicated for 30 min. The resulting milky colloidal suspension is centrifugated for 20 min at 3000 rpm and the supernatant solution containing the exfoliated material is recovered. The successful exfoliation is proven by the Tyndall effect exhibited by the solution with the assistance of a laser beam (Figure 4d).

3.2. Crystal Structure Analyses

Singe-crystal X-ray diffraction data have been collected on a Bruker ApexII CCD diffractometer using graphite-monochromated Mo Kα radiation (λ = 0.71073 Å). Low-temperature data collections have been performed employing a Cryostream 600 (Oxford Cryosystems). For all the species, a full sphere of the reciprocal space has been collected, granting data completeness up to at least $(\sin\theta)/\lambda$ = 0.6 $Å^{-1}$. CCDC 2156201–2156204 contain the supplementary crystallographic data for the paper. These data can be obtained free of charge from the Cambridge Crystallographic Data Center.

3.2.1. Crystal Data for $3H_3L^1\cdot 2DMSO\cdot 4H_2O$

$C_{55}H_{56}N_{24}O_{12}S_2$, M_r = 1309.35 g mol^{-1}, monoclinic, space group $C2/c$ (No. 15), a = 10.6817(13), b = 11.9280(15), c = 46.127(6) Å, β = 91.586(2)°, V = 5874.9(13) $Å^3$, Z = 4, d_{calc} = 1.480 g cm^{-3}, T = 120(2) K, crystal size = 0.200 × 0.120 × 0.040 mm^3, μ = 0.176 mm^{-1}. Refinement of 426 parameters on 6586 independent reflections out of 20559 measured reflections (R_{int} = 0.0716, R_σ = 0.1132, $2\theta_{max}$ = 56.8°) led to R_1 = 0.0834 [$I > 2\sigma(I)$], wR_2 = 0.1886 (all data), and S = 1.076, with the largest peak and hole of 0.352 and −0.492 e $Å^{-3}$. All the non-hydrogen atoms were given anisotropic displacement parameters. Water molecules were refined as rigid groups. All the hydrogen atoms were clearly seen in a difference Fourier map; they were added in idealized positions and refined by riding on their parent atom with an isotropic displacement parameter 1.2 (or 1.5) times that of the pertinent parent atom. Hydrogen atoms of the enolate moieties were refined as disordered over two positions.

3.2.2. Crystal Data for $H_2\mathbf{L^2}$

$C_{16}H_{12}N_4O_2$, M_r = 292.30 g mol^{-1}, monoclinic, space group $P2_1/c$ (No. 14), a = 8.0327(13), b = 6.5161(10), c = 25.339(4) Å, β = 93.530(2)°, V = 1323.8(4) Å^3, Z = 4, d_{calc} = 1.467 g cm^{-3}, T = 295(2) K, crystal size = 0.600 × 0.500 × 0.140 mm^3, μ = 0.101 mm^{-1}. Refinement of 200 parameters on 4174 independent reflections out of 28885 measured reflections (R_{int} = 0.0202, R_σ = 0.0126, $2\theta_{max}$ = 63.0°) led to R_1 = 0.0504 [$I > 2\sigma(I)$], wR_2 = 0.1429 (all data), and S = 1.082, with the largest peak and hole of 0.337 and −0.220 e Å^{-3}. All the non-hydrogen atoms were given anisotropic displacement parameters. All the hydrogen atoms were clearly seen in a difference Fourier map; they were added in idealized positions and refined by riding on their parent atom with an isotropic displacement parameter 1.2 (or 1.5) times that of the pertinent parent atom. Hydrogen atoms of the enolate and 1*H*-tetrazol-5-yl moieties were refined as disordered over two positions.

3.2.3. Crystal Data for $[NEt_4]_3[Fe(H\mathbf{L^1})_3]\cdot 3THF$ (**1**)

$C_{87}H_{114}FeN_{27}O_9$, M_r = 1737.90 g mol^{-1}, triclinic, space group P–1 (No. 2), a = 15.3612(12), b = 16.5594(12), c = 19.5708(15) Å, α = 65.652(1), β = 80.305(1), γ = 86.363(1)°, V = 4470.6(6) Å^3, Z = 2, d_{calc} = 1.291 g cm^{-3}, T = 150(2) K, crystal size = 0.300 × 0.120 × 0.090 mm^3, μ = 0.241 mm^{-1}. Refinement of 1012 parameters (applying 339 restraints) on 18277 independent reflections out of 52987 measured reflections (R_{int} = 0.0830, R_σ = 0.1135, $2\theta_{max}$ = 52.7°) led to R_1 = 0.0752 [$I > 2\sigma(I)$], wR_2 = 0.2473 (all data), and S = 1.012, with the largest peak and hole of 0.750 and −0.546 e Å^{-3}. All the non-hydrogen atoms (apart from the disordered carbon atoms of the cations) were given anisotropic displacement parameters. The hydrogen atoms of the iron complex were clearly seen in a difference Fourier map. All the hydrogen atoms were added in idealized positions and refined by riding on their parent atom with an isotropic displacement parameter 1.2 (or 1.5) times that of the pertinent parent atom. Hydrogen atoms on the tetrazole ring of the dianionic ligands $(H\mathbf{L^1})^{2-}$ were refined as disordered over two positions: atom N^1 of a ring and atom N^2 of the other. Some of the tetraethylammonium cations were refined by restraining equivalent 1,2 (and 1,3) distances to be equal. The three THF molecules were found to be heavily disordered in the channels running along the (**c** – **a**) direction. Since it was impossible to refine a discrete model for the disorder components, the contribution of the solvent molecules to the calculated structure factors was determined according to the SQUEEZE procedure [42].

3.2.4. Crystal Data for $[Zn\mathbf{L^2}(DMSO)]$ (**2**)

$C_{18}H_{16}N_4O_3SZn$, M_r = 433.78 g mol^{-1}, monoclinic, space group $P2_1/n$ (No. 14), a = 10.8689(12), b = 14.8447(16), c = 12.5011(14) Å, β = 113.076(1)°, V = 1855.6(4) Å^3, Z = 4, d_{calc} = 1.553 g cm^{-3}, T = 295(2) K, crystal size = 0.200 × 0.016 × 0.010 mm^3, μ = 1.463 mm^{-1}. Refinement of 248 parameters (applying 8 restraints) on 3301 independent reflections out of 17673 measured reflections (R_{int} = 0.0672, R_σ = 0.0528, $2\theta_{max}$ = 50.3°) led to R_1 = 0.0625 [$I > 2\sigma(I)$], wR_2 = 0.1921 (all data), and S = 1.037, with the largest peak and hole of 0.939 and −0.839 e Å^{-3}. All the non-hydrogen atoms were given anisotropic displacement parameters. All the hydrogen atoms were clearly seen in a difference Fourier map; they were added in idealized positions and refined by riding on their parent atom with an isotropic displacement parameter 1.2 (or 1.5) times that of the pertinent parent atom. The sulphur atom of the coordinate DMSO molecule was refined as disordered over two positions, corresponding to its pyramidal inversion. Soft restraints on equivalent 1,2 and 1,3 distances of the two disordered components were applied.

4. Conclusions

In conclusion, we reported the synthesis and characterization of two new mixed-donor ligands combining a chelating β-diketone group with tetrazolyl fragments. Their reactivity towards different metal salts has been explored, evidencing the obtainment of tris–chelate complexes with peripheral tetrazolyl groups. The low solubility and easy rearrangement of these chelate complexes in the solution make their crystallization and successive use in networking towards heterometallic structures difficult. Despite this, we succeeded in

isolating single crystals of an anionic Fe(III) tris–chelate complex, showing in the solid state a self-catenated 2D supramolecular framework through pseudo-rotaxane links. The concomitant use of both donor groups by κ^2O,O' chelation and μ-κN^2:κN^3 is realized in the 2D homometallic coordination polymer [Zn$\mathbf{L^2}$(DMSO)] with **sql** topology. The Zn(II) species is luminescent in the solid state, with an emission red-shifted with respect to the free ligand, and interestingly, it can be easily exfoliated in water. Here, reported results highlight the potential of exploiting a new class of linkers containing the chelating β-diketonate group, to better control the stereochemistry of the metal atoms and tetrazolyl fragments, which give networking through coordinative or hydrogen bonding.

Supplementary Materials: The following supporting information can be downloaded at: https://www.mdpi.com/article/10.3390/inorganics10040055/s1, Figures S1 and S2: FT-IR spectra; Figures S3–S8: 1H and 13C NMR spectra; Figures S9 and S10: UV-vis spectra; Figures S11 and S12: further plots of the crystal structures, CIF files 2156201 ($3H_3\mathbf{L^1}\cdot 2DMSO\cdot 4H_2O$), 2156202 ($H_2\mathbf{L^2}$), 2156203 (**1**) and 2156204 (**2**).

Author Contributions: Conceptualization, funding acquisition and supervision, L.C.; investigation, D.B., L.C. and P.M.; data curation, P.M.; writing—original draft preparation and writing—review and editing, L.C. and P.M. All authors have read and agreed to the published version of the manuscript.

Funding: This research was funded by Università degli Studi di Milano (PSR2019_DIP_005_PI_LCAR).

Institutional Review Board Statement: Not applicable.

Informed Consent Statement: Not applicable.

Acknowledgments: The authors thank Elena Cariati and Daniele Malpicci for the photoluminescence measurements.

Conflicts of Interest: The authors declare no conflict of interest.

References

1. Batten, S.R.; Champness, N.R.; Chen, X.-M.; Garcia-Martinez, J.; Kitagawa, S.; Öhrström, L.; O'Keeffe, M.; Suh, M.P.; Reedijk, J. Terminology of metal–organic frameworks and coordination polymers (IUPAC Recommendations 2013). *Pure Appl. Chem.* **2013**, *85*, 1715. [CrossRef]
2. Batten, S.R.; Champness, N.R.; Chen, X.-M.; Garcia-Martinez, J.; Kitagawa, S.; Öhrström, L.; O'Keeffe, M.; Suh, M.P.; Reedijk, J. Coordination polymers. *CrystEngComm* **2012**, *14*, 3001. [CrossRef]
3. Yaghi, O.M.; Kalmutzki, M.J.; Diercks, C.S. *Introduction to Reticular Chemistry: Metal-Organic Frameworks and Covalent Organic Frameworks*; Wiley-VCH: Weinheim, Germany, 2019.
4. Batten, S.R.; Neville, S.M.; Turner, D.R. *Coordination Polymers: Design, Analysis and Application*; Springer: New York, NY, USA, 2010.
5. Kaskel, S. (Ed.) *The Chemistry of Metal-Organic Frameworks: Synthesis, Characterization, and Applications*; Wiley-VCH: Weinheim, Germany, 2016.
6. Öhrström, L.; Amombo Noa, F.M. *Metal-Organic Frameworks*; American Chemical Society: Washington, DC, USA, 2021. [CrossRef]
7. Ye, Y.; Xian, S.; Cui, H.; Tan, K.; Gong, L.; Liang, B.; Pham, T.; Pandey, H.; Krishna, R.; Lan, P.C.; et al. Metal–organic framework based hydrogen-bonding nanotrap for efficient acetylene storage and separation. *J. Am. Chem. Soc.* **2022**, *144*, 1681. [CrossRef] [PubMed]
8. Li, H.; Wang, K.; Sun, Y.; Lollar, C.T.; Li, J.; Zhou, H.-C. Recent advances in gas storage and separation using metal–organic frameworks. *Mater. Today* **2018**, *21*, 108. [CrossRef]
9. Yang, D.; Gates, B.C. Catalysis by metal organic frameworks: Perspective and suggestions for future research. *ACS Catal.* **2019**, *9*, 1779. [CrossRef]
10. Farrusseng, D.; Aguado, S.; Pinel, C. MOFs in catalysis. *Angew. Chem. Int. Ed.* **2009**, *48*, 7502. [CrossRef]
11. Hu, Z.; Deibert, B.J.; Li, J. Luminescent metal–organic frameworks for chemical sensing and explosive detection. *Chem. Soc. Rev.* **2014**, *43*, 5815. [CrossRef]
12. Horcajada, P.; Gref, R.; Baati, T.; Allan, P.K.; Maurin, G.; Couvreur, P.; Férey, G.; Morris, R.E.; Serre, C. Metal–organic frameworks in biomedicine. *Chem. Rev.* **2012**, *112*, 1232. [CrossRef]
13. Ding, M.; Flaig, R.W.; Jiang, H.L.; Yaghi, O.M. Carbon capture and conversion using metal–organic frameworks and MOF-based materials. *Chem. Soc. Rev.* **2019**, *48*, 2783. [CrossRef]
14. Rojas, S.; Horcajada, P. Metal–organic frameworks for the removal of emerging organic contaminants in water. *Chem. Rev.* **2020**, *120*, 8378. [CrossRef]

15. Kobielska, P.A.; Howarth, A.J.; Farha, O.K.; Nayak, S. Metal–organic frameworks for heavy metal removal from water. *Coord. Chem. Rev.* **2018**, *358*, 92. [CrossRef]
16. Kim, H.; Yang, S.; Rao, S.R.; Narayanan, S.; Kapustin, E.A.; Furukawa, H.; Umans, A.S.; Yaghi, O.M.; Wang, E.N. Water harvesting from air with metal–organic frameworks powered by natural sunlight. *Science* **2017**, *356*, 430. [CrossRef] [PubMed]
17. Zhang, J.-P.; Zhang, Y.-B.; Lin, J.-B.; Chen, X.-M. Metal azolate frameworks: From crystal engineering to functional materials. *Chem. Rev.* **2012**, *112*, 1001. [CrossRef] [PubMed]
18. Masciocchi, N.; Galli, S.; Colombo, V.; Maspero, A.; Palmisano, G.; Seyyedi, B.; Lamberti, C.; Bordiga, S. Cubic octanuclear Ni(II) clusters in highly porous polypyrazolyl-based materials. *J. Am. Chem. Soc.* **2010**, *132*, 7902. [CrossRef]
19. Wang, K.; Lv, X.-L.; Feng, D.; Li, J.; Chen, S.; Sun, J.; Song, L.; Xie, Y.; Li, J.-R.; Zhou, H.-C. Pyrazolate-based porphyrinic metal–organic framework with extraordinary base-resistance. *J. Am. Chem. Soc.* **2016**, *138*, 914. [CrossRef]
20. Ostrovskii, V.A.; Trifonov, R.E.; Popova, E.A. Medicinal chemistry of tetrazoles. *Russ. Chem. Bull.* **2012**, *61*, 768. [CrossRef]
21. Frija, L.M.T.; Ismael, A.; Cristiano, M.L.S. Photochemical transformations of tetrazole derivatives: Applications in organic synthesis. *Molecules* **2010**, *15*, 3757. [CrossRef]
22. Fischer, D.; Klapötke, T.M.; Stierstorfer, J. 1,5-Di(nitramino)tetrazole: High sensitivity and superior explosive performance. *Angew. Chem. Int. Ed.* **2015**, *54*, 10299. [CrossRef]
23. Zhao, H.; Qu, Z.-R.; Ye, H.-Y.; Xiong, R.-G. In situ hydrothermal synthesis of tetrazole coordination polymers with interesting physical properties. *Chem. Soc. Rev.* **2008**, *37*, 84. [CrossRef]
24. Dinca, M.; Yu, A.F.; Long, J.R. Microporous metal−organic frameworks incorporating 1,4-benzeneditetrazolate: Syntheses, structures, and hydrogen storage properties. *J. Am. Chem. Soc.* **2006**, *128*, 8904. [CrossRef]
25. Tabacaru, A.; Pettinari, C.; Galli, S. Coordination polymers and metal–organic frameworks built up with poly(tetrazolate) ligands. *Coord. Chem. Rev.* **2018**, *372*, 1. [CrossRef]
26. Demko, Z.P.; Sharpless, K.B. Preparation of 5-substituted 1-tetrazoles from nitriles in water. *J. Org. Chem.* **2001**, *66*, 7945. [CrossRef] [PubMed]
27. Wen, T.; Zhou, X.-P.; Zhang, D.-X.; Li, D. Luminescent mechanochromic porous coordination polymers. *Chem.—Eur. J.* **2014**, *20*, 644. [CrossRef]
28. Liu, Z.-F.; Wu, M.-F.; Zheng, F.-K.; Wang, S.-H.; Zhang, M.-J.; Chen, J.; Xiao, Y.; Guo, G.-C.; Wua, A.-Q. Zn(II) coordination compound based on in situ generated 3-(5*H*-tetrazol)benzaldehyde with diverse modes: Hydrothermal synthesis, crystal structures and photoluminescent properties. *CrystEngComm* **2013**, *15*, 7038. [CrossRef]
29. Li, N.; Chang, Z.; Huang, H.; Feng, R.; He, W.-W.; Zhang, M.; Madden, D.G.; Zaworotko, M.J.; Bu, X.-H. Specific K^+ binding sites as CO_2 traps in a porous MOF for enhanced CO_2 selective sorption. *Small* **2019**, *15*, 1900426. [CrossRef]
30. Ji, L.-Q.; Yang, J.; Zhang, Z.-Y.; Qian, Y.; Su, Z.; Han, M.; Liu, H.-K. Enhanced catalytic performance for oxygen reduction reaction derived from nitrogen-rich tetrazolate-based heterometallic metal–organic frameworks. *Cryst. Growth Des.* **2019**, *19*, 2991. [CrossRef]
31. Nunes, M.S.; Gomes, D.M.; Gomes, A.C.; Neves, P.; Mendes, R.F.; Paz, F.A.A.; Lopes, A.D.; Valente, A.A.; Gonçalves, I.S.; Pillinger, M. A 5-(2-pyridyl)tetrazolate complex of molybdenum(VI), its structure, and transformation to a molybdenum oxide-based hybrid heterogeneous catalyst for the epoxidation of olefins. *Catalysts* **2021**, *11*, 1407. [CrossRef]
32. Carlucci, L.; Ciani, G.; Maggini, S.; Proserpio, D.M.; Visconti, M. Heterometallic modular metal–organic 3d frameworks assembled via new tris-β-diketonate metalloligands: Nanoporous materials for anion exchange and scaffolding of selected anionic guests. *Chem.—Eur. J.* **2010**, *16*, 12328. [CrossRef]
33. Visconti, M.; Maggini, S.; Ciani, G.; Mercandelli, P.; del Secco, B.; Prodi, L.; Sgarzi, M.; Zaccheroni, N.; Carlucci, L. New lanthanide metalloligands and their use for the assembly of Ln−Ag bimetallic coordination frameworks: Stepwise modular synthesis, structural characterization, and optical properties. *Cryst. Growth Des.* **2019**, *19*, 5376. [CrossRef]
34. Amantini, D.; Beleggia, R.; Fringuelli, F.; Pizzo, F.; Vaccaro, L. TBAF-catalyzed synthesis of 5-substituted 1-tetrazoles under solventless conditions. *J. Org. Chem.* **2004**, *69*, 2896. [CrossRef]
35. Rasmussen, S.; Tunnicliff, D.D.; Brattain, R.R. Infrared and Ultraviolet spectroscopic studies on ketones. *J. Am. Chem. Soc.* **1949**, *71*, 1068. [CrossRef]
36. Mosalkova, A.P.; Voitekhovich, S.V.; Lyakhov, A.S.; Ivashkevich, L.S.; Gaponik, P.N.; Ivashkevich, O.A. Direct Synthesis and characterization of new copper(II) and zinc(II) 5-R-tetrazolato complexes [R = Me, Ph, 4-Py] with ethylenediamine and DMSO as coligands. *Z. Anorg. Allg. Chem.* **2012**, *638*, 103. [CrossRef]
37. Meza-Morales, W.; Estévez-Carmona, M.M.; Alvarez-Ricardo, Y.; Obregón-Mendoza, M.A.; Cassani, J.; Ramírez-Apan, M.T.; Escobedo-Martínez, C.; Soriano-García, M.; Reynolds, W.F.; Enríquez, R.G. Full structural characterization of homoleptic complexes of diacetylcurcumin with Mg, Zn, Cu, and Mn: Cisplatin-level cytotoxicity in vitro with minimal acute toxicity in vivo. *Molecules* **2019**, *24*, 1598. [CrossRef] [PubMed]
38. Hansen, P.E. Structural studies of β-diketones and their implications on biological effects. *Pharmaceuticals* **2021**, *14*, 1189. [CrossRef] [PubMed]
39. Calligaris, M.; Carugo, O. Structure and bonding in metal sulfoxide complexes. *Coord. Chem. Rev.* **1996**, *153*, 83. [CrossRef]

40. Calligaris, M. Structure and bonding in metal sulfoxide complexes: An update. *Coord. Chem. Rev.* **2004**, *248*, 351. [CrossRef]
41. Li, Y.-Z.; Fu, Z.-H.; Xu, G. Metal–organic framework nanosheets: Preparation and applications. *Coord. Chem. Rev.* **2019**, *388*, 79. [CrossRef]
42. Spek, A.L. PLATON SQUEEZE: A tool for the calculation of the disordered solvent contribution to the calculated structure factors. *Acta Crystallogr. Sect. C Struct. Chem.* **2015**, *71*, 9. [CrossRef]